Supplementary information

Alteration of Oxygen Evolution Mechanisms in Layered $LiCoO_2$ Structures by Intercalation of Alkali Metal Ions

Yohan Kim[a], Seongmin Kim[b], Minyoung Shim[a], Yusik Oh[a], Kug-Seung Lee[c], Yousung Jung[b], and Hye Ryung Byon[a]*

[a] Department of Chemistry, Korea Advanced Institute of Science and Technology (KAIST), 291, Daehak-ro, Yuseong-gu, Daejeon 34141, Republic of Korea

[b] Department of Chemical and Biomolecular Engineering, Korea Advanced Institute of Science and Technology (KAIST), 291 Daehak-ro, Yuseong-gu, Daejeon 34141, Republic of Korea

[c] Pohang Accelerator Laboratory, 80 Jigok-ro 127 beon-gil, Pohang, Gyeongbuk 37673, Republic of Korea

* E-mail: hrbyon@kaist.ac.kr

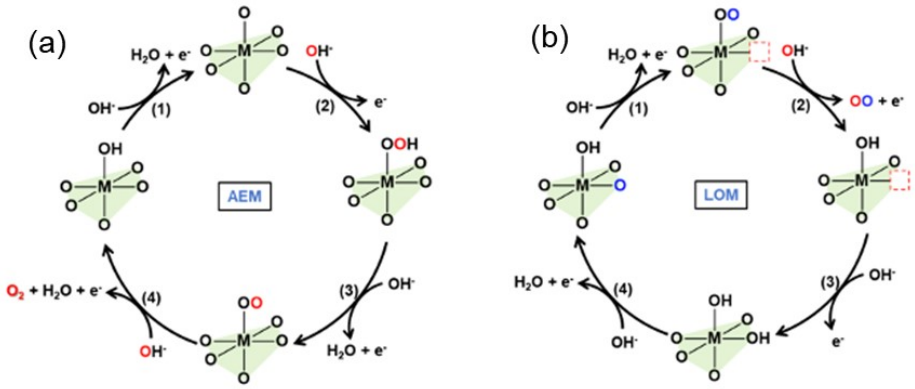

Figure S1. Two OER processes, (a) absorbate evolution mechanism and (b) lattice oxygen mechanism.

Table S1. Summary of recent studies about OER activity of $LiCoO_2$ related electrocatalyst

OER catalyst	Electrolyte solution	Substrate	Overpotential @ 10 mA cm^{-2} (mV)	Tafel slope (mV dec^{-1})	References
Layered $LiCoO_2$	0.1 M LiOH	Glassy carbon disk electrode	440	80.8	**This work**
	0.1 M NaOH		448	66.2	
	0.1 M KOH		416	60.0	
	0.1 M CsOH		392	47.1	
Delithiated Layered $LiCoO_2$	0.1 M KOH	Carbon fiber paper	390	57	*J. Am. Chem. Soc.*, 2017, **139**, 6270-6276 [1]
Spinel $Li_2Co_2O_4$	O_2 saturated 1 M KOH	Carbon fiber paper	361	46	*ACS Catal.*, 2019, **9**, 7389-7397 [2]
Layered $LiCoO_2$ nanosheet	0.1 M KOH	Glassy carbon disk electrode	410	88	*ACS Appl. Mater. Interfaces.*, 2017, **9**, 7100-7107 [3]
La-doped layered $LiCoO_2$	O_2 saturated 0.1 M KOH	Glassy carbon disk electrode	330	48	*Nano Lett.*, 2019, **19**, 8774-8779 [4]
Layered $LiCo_{0.8}Fe_{0.2}O_2$	0.1 M KOH	Glassy carbon disk electrode	340	50	*Adv. Mater.*, 2015, **27**, 7150-7155 [5]
Layered $LiCoO_{1.8}Cl_{0.2}$	1 M KOH	Glassy carbon disk electrode	270	55.4	*Nat. Catal.*, 2021, **4**, 212–222 [6]
Layered Li_2IrO_3	0.1 M KOH	Glassy carbon disk electrode	290	50	*Nat. Commun.*, 2020, **11**, 1378 [7]
	0.1 M NaOH		340	70	

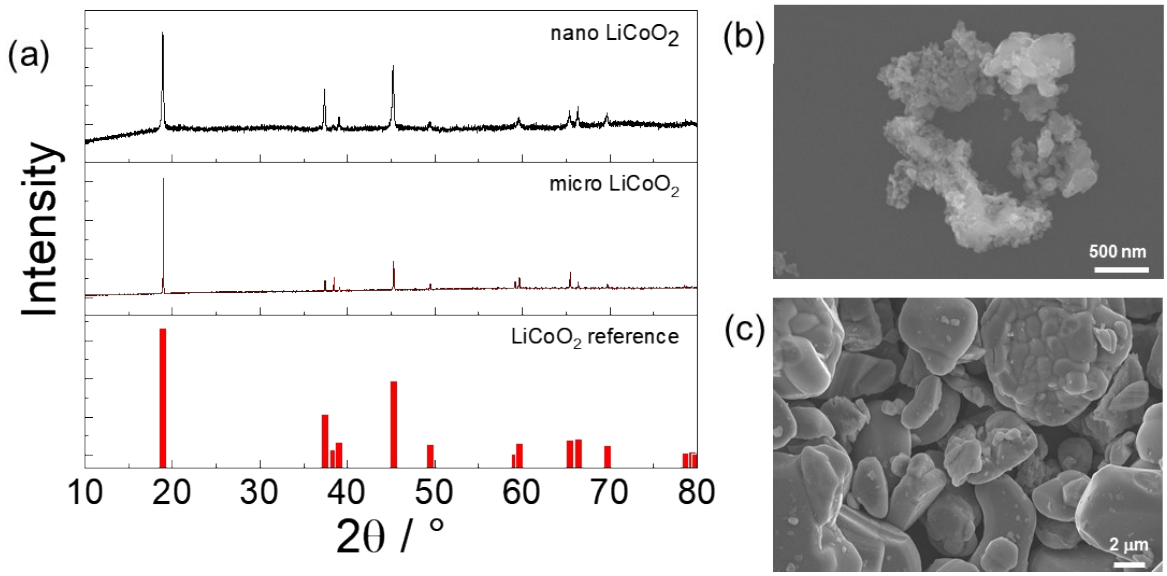

Figure S2. Structural characterizations of n-LCO and m-LCO. (a) Powder XRD patterns of n-LCO (top), m-LCO (middle), and reference of layered LCO (bottom, ICDD 00-050-0653). XRD analysis revealed a marginal impurity phase for all LCO samples. (b–c) SEM images of (b) n-LCO and (c) m-LCO. The sizes of n-LCO and m-LCO were 10~100 nm and 10~20 μm, respectively.

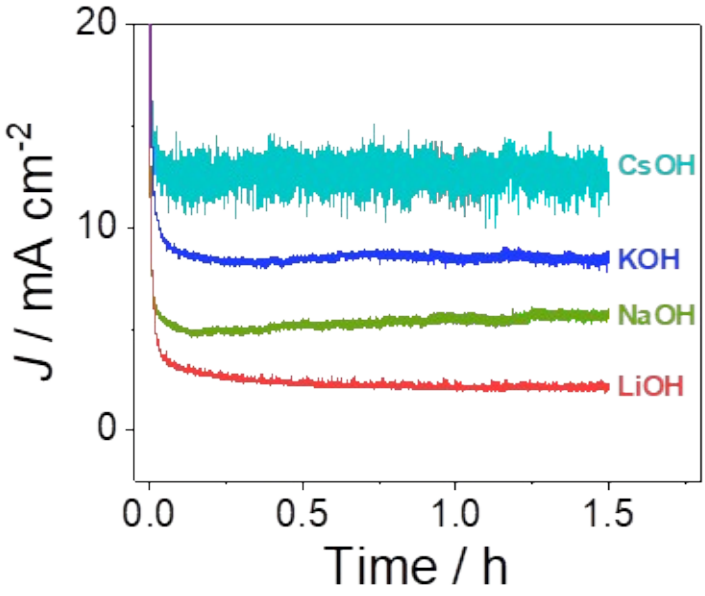

Figure S3. Chronoamperometry of m-LCO at 1.66 V vs. RHE for 90 min. Among 0.1 M LiOH, NaOH, KOH, and CsOH solution, the m-LCO with CsOH showed the highest current density at 13 mA cm^{-2} throughout 90 min OER performances.

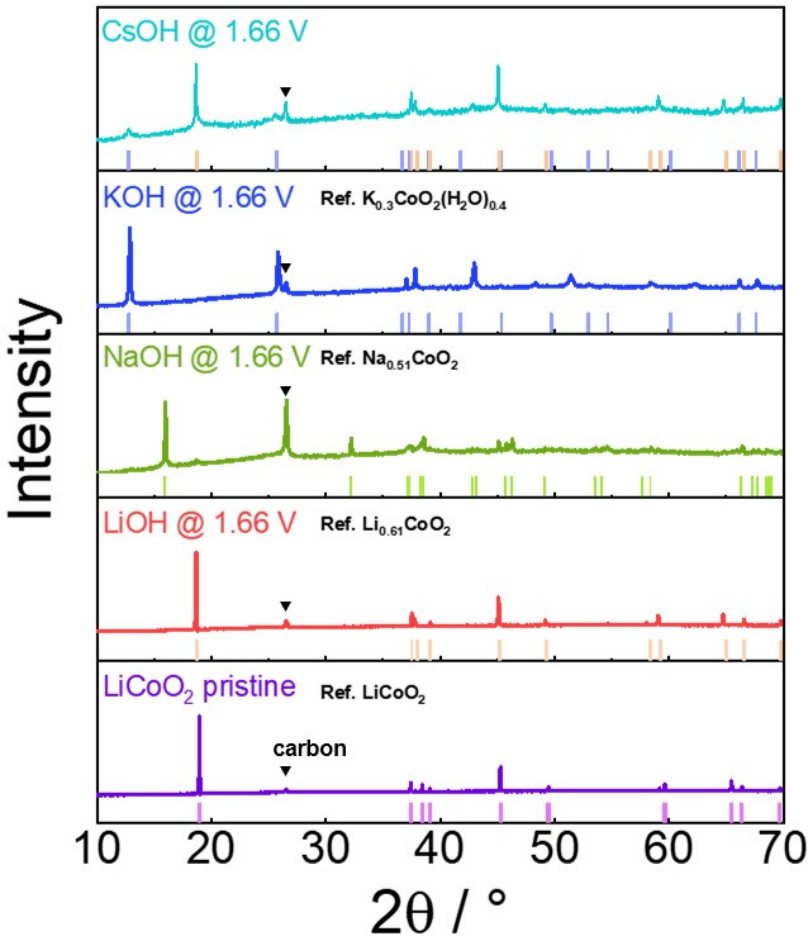

Figure S4. Wide-angle views of powder XRD patterns of pristine m-LCO and the m-LCOs after 90 min of OER at 1.66 V vs. RHE with LiOH, NaOH, KOH, and CsOH (from bottom to top). Corresponding bar patterns are references of the layered LCO, $Li_{0.61}CoO_2$ (ICDD 01-080-4976), $Na_{0.51}CoO_2$ (ICDD 01-075-7656), $K_{0.3}CoO_2(H_2O)_{0.4}$ (ICDD 01-074-9522), and the combination of $Li_{0.61}CoO_2$ and $K_{0.3}CoO_2(H_2O)_{0.4}$, respectively (from bottom to top). The inverse triangles indicate carbon paper.

There were entire structural transformations by intercalation of the hydrated Na^+ and K^+ into the delithiated LCOs. However, we could not find any references having identical XRD patterns of our catalyst samples. At high-angle regions, the XRD patterns of Na^+- and K^+-intercalated LCOs did not overlap with $Na_{0.51}CoO_2$ and $K_{0.3}CoO_2(H_2O)_{0.4}$, respectively, due to the significantly remaining Li^+. The m-LCO with CsOH preserved the original LCO structure, while the small signal at 12.7° demonstrated minute intercalation of hydrated Cs^+.

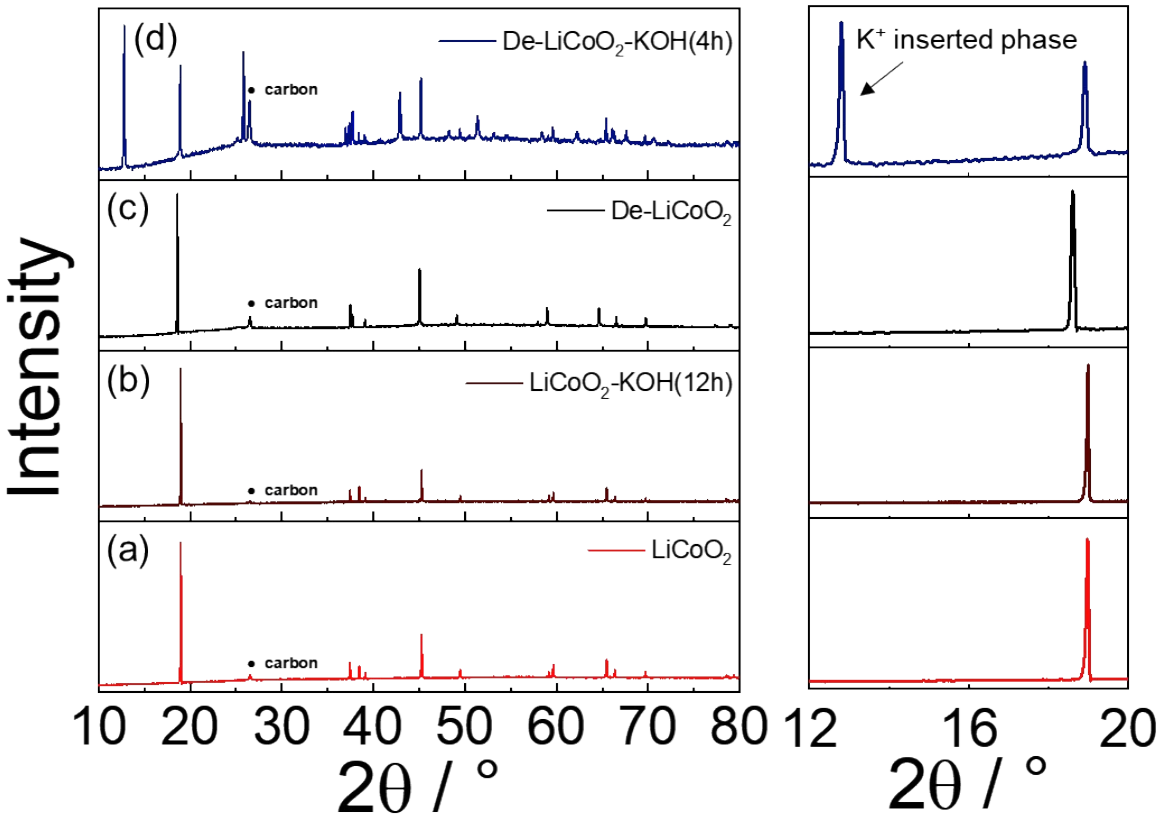

Figure S5. XRD patterns of m-LCO soaked in 0.1 M KOH(aq) for 4 h without any external bias. The left and right panels are wide-angle view (10~80°) and the high-magnification region at 12~20° region, respectively. (a) Pristine m-LCO and (b) m-LCO soaked in 0.1 M KOH(aq) for 12 h without delithiation. There was no change in XRD patterns. (c) Delithiated m-LCO, prepared by applying a constant current of 1.6 mA until the charging potential was increased to 0.95 V vs. Ag/AgCl in 0.5 M Li_2SO_4(aq). The 003 reflection at 18.9° was shifted to 18.6° due to the electrostatic repulsion of CoO_2 layers.[8] (d) Delithiated m-LCO immersed in 0.1 M KOH(aq) for 4 h. The intense peak appeared at 13°, the same as the one after 90 min OER test (**Figure S4**), suggesting the insertion of K^+ through the capillary force. All XRD patterns of the original LCO were maintained in the absence of anodic reactions. In addition, we observed that the 003 reflection of the LCO was shifted to the original position once K^+ was inserted. Presumably, Li^+ ions were re-distributed across the LCO to form thermodynamically stable structures.

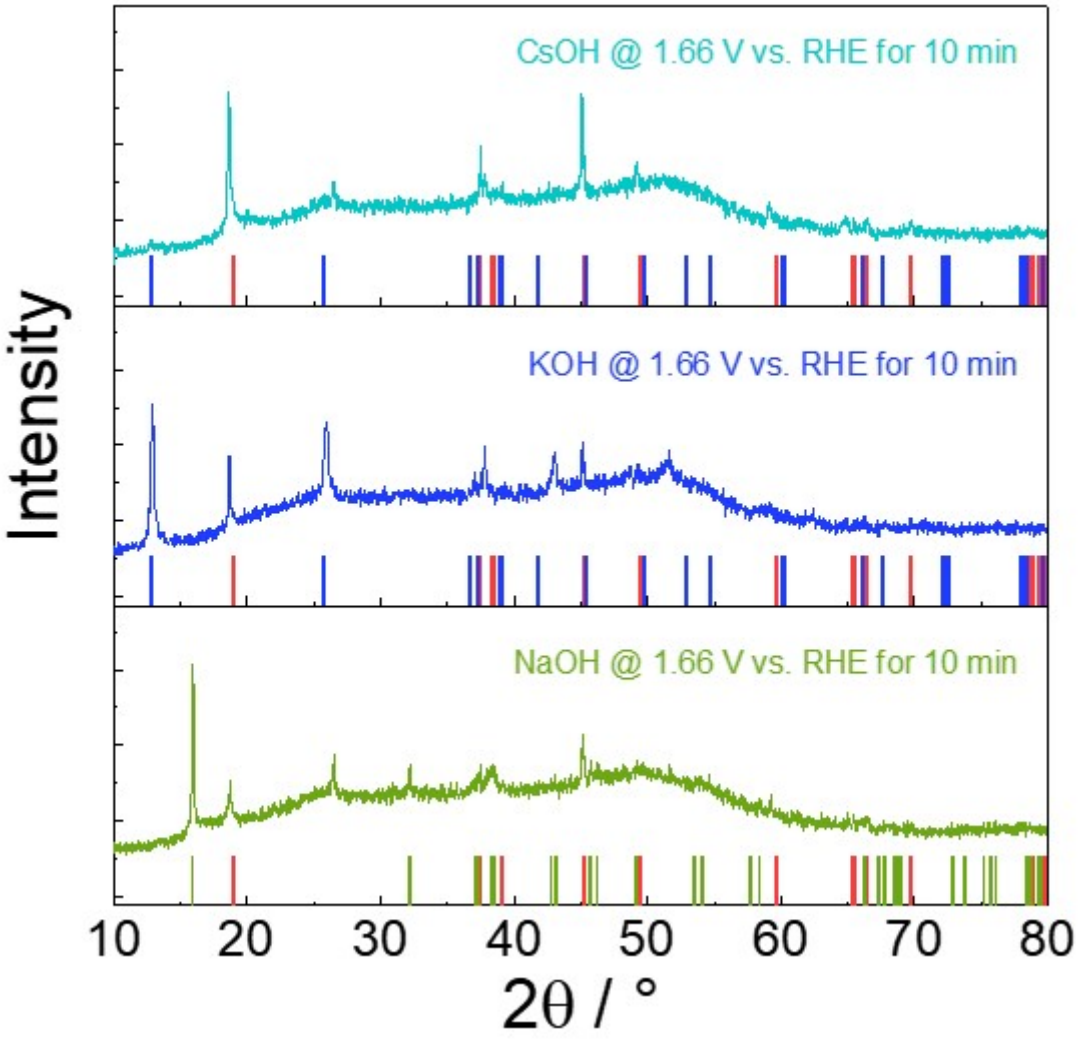

Figure S6. Powder XRD patterns of m-LCO after 10 min of OER at 1.66 V vs. RHE. Bar patterns are references of the layered LCO (red) in all panels, $Na_{0.51}CoO_2$ (green) in the NaOH panel, and $K_{0.3}CoO_2(H_2O)_{0.4}$ (blue) in the KOH and CsOH panels. While all XRD patterns were similar to the ones after 90 min OER (**Figure S4**), the 003 reflections of the LCOs were still maintained. The broad hills over the baselines also indicated incomplete structure transformations at the short period of OER.

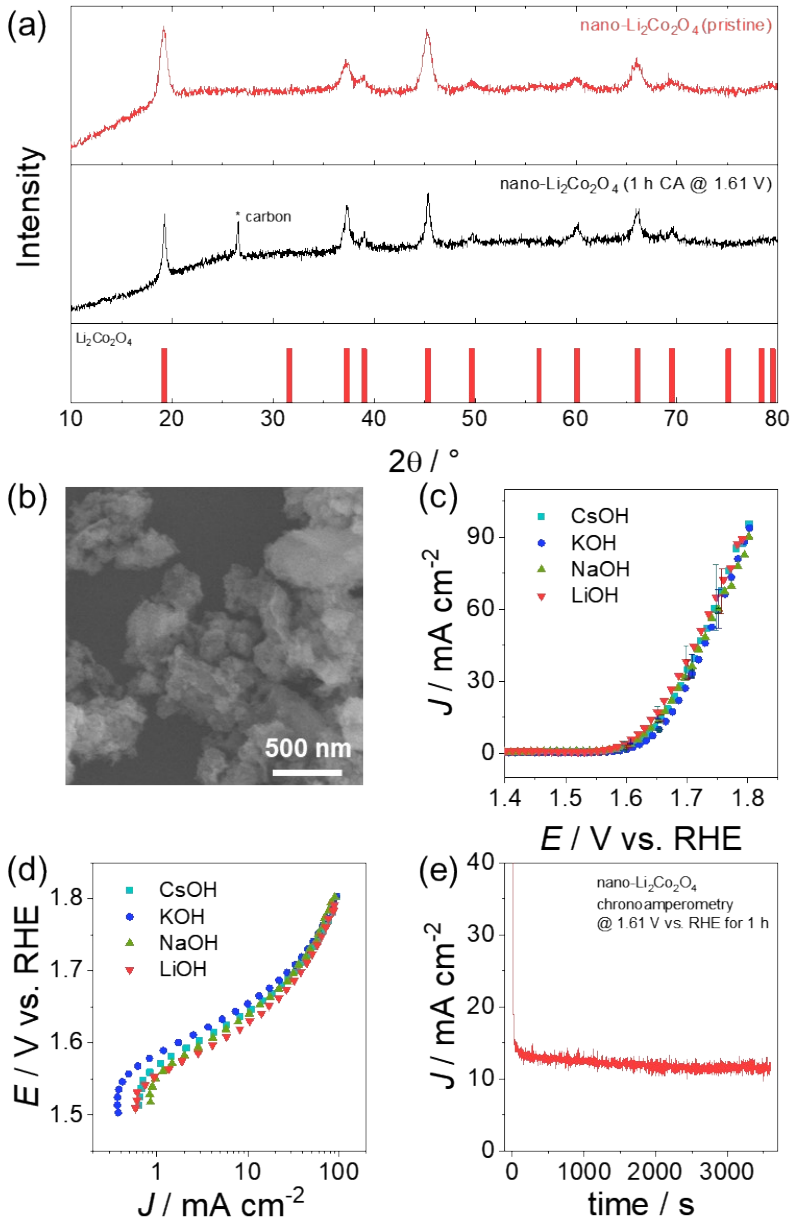

Figure S7. Characteristics of nano spinel $Li_2Co_2O_4$ and OER performances with various electrolyte solutions. (a) Powder XRD pattern of pristine $Li_2Co_2O_4$, the one after OER at 1.61 V vs. RHE for 60 min, and the reference of spinel $Li_2Co_2O_4$ (ICDD 01-082-0342).[9] The spinel $Li_2Co_2O_4$ has a single peak at 2θ = 66 ° and is distinct from doublet signals of the layered LCO.[9-11] (b) SEM image of pristine nano $Li_2Co_2O_4$. (c) OER polarization curves, (d) corresponding Tafel plots with 0.1 M LiOH, NaOH, KOH, and CsOH solution, and (e) chronoamperometry test at 1.61 V vs. RHE for 60 min with KOH. The data were acquired from three $Li_2Co_2O_4$ samples at each solution. Mass loading of $Li_2Co_2O_4$ was ~0.08 mg_{oxide} cm^{-2} on the GC electrode. The spinel nano-$Li_2Co_2O_4$ showed negligible electrolyte effects for OER tests.

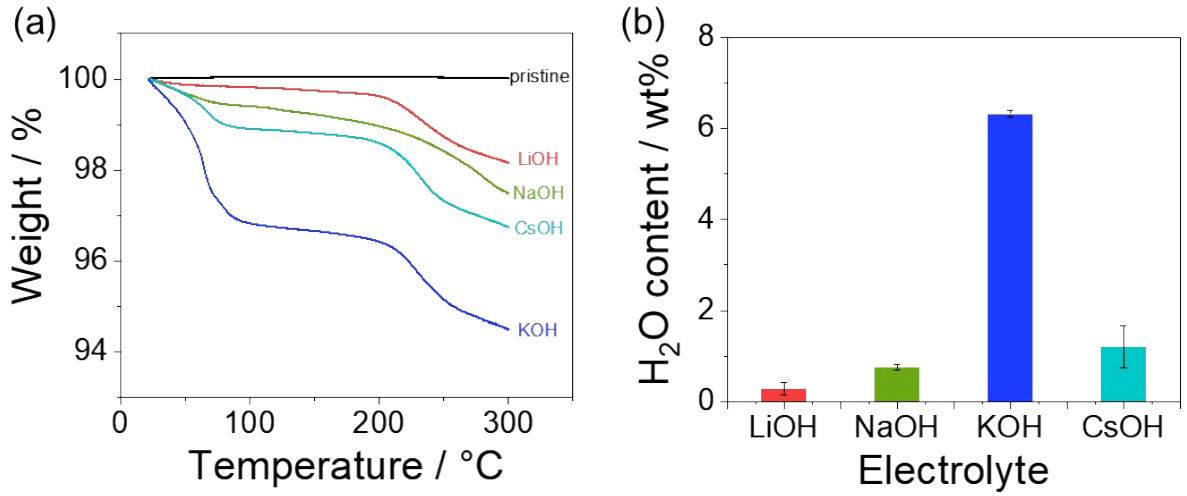

Figure S8. TGA of m-LCOs after OER tests to measure H_2O contents. (a) Representative TGA curves of m-LCO after 90 min of OER at 1.66 V vs. RHE with different electrolyte solutions. TGA curves were acquired with N_2 flow of 100 mL min^{-1} and a ramping rate of 0.25 °C min^{-1}. (b) Estimated average H_2O wt% from three measurements. The water contents were 0.28 ± 0.13, 0.76 ± 0.06, 6.32 ± 0.07, and 1.20 ± 0.45 wt% for LiOH, NaOH, KOH, and CsOH solution, respectively.

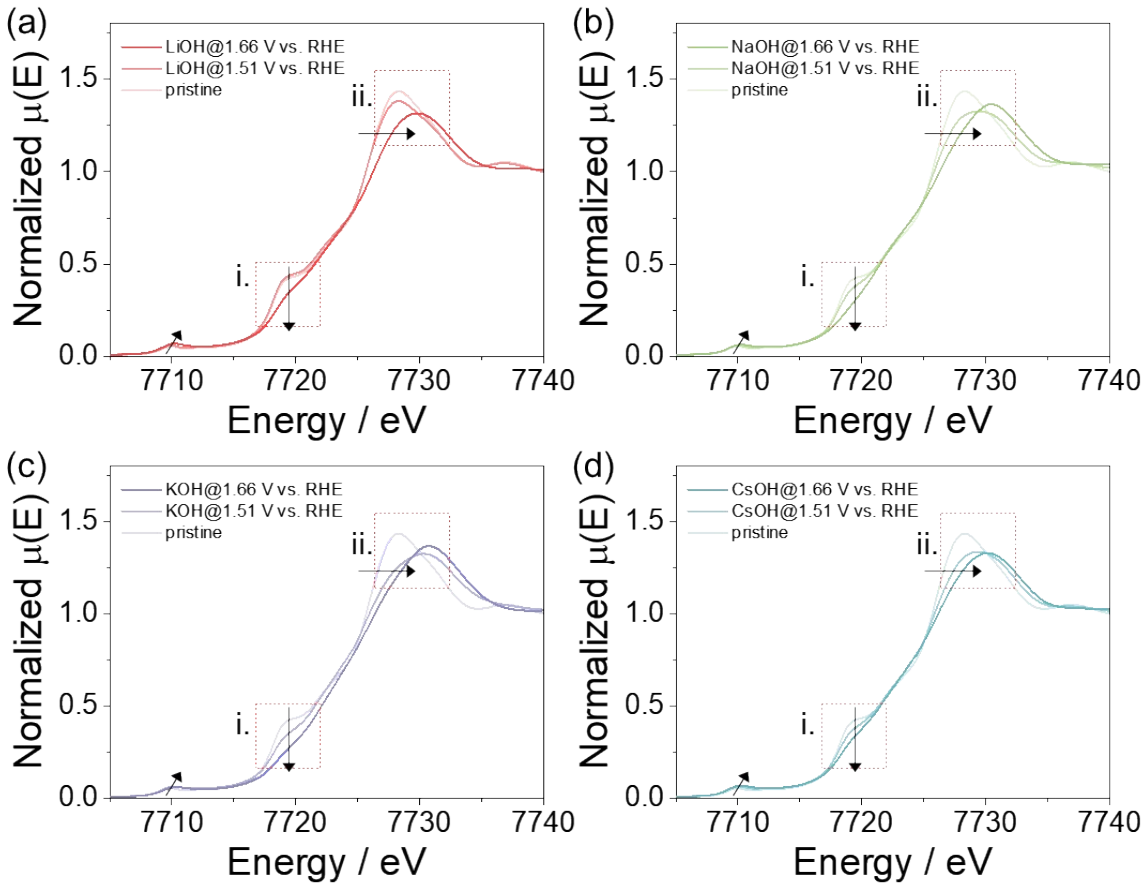

Figure S9. *Ex situ* XANES spectra of m-LCOs at Co *K* edge region with the transmission mode. OER tests were conducted at 1.51 V and 1.66 V vs. RHE for 60 min. The electrolyte solutions were 0.1 M of (a) LiOH, (b) NaOH, (c) KOH, and (d) CsOH. With increasing anodic potentials from 1.51 V (onset OER potential) to 1.66 V (~10 mA cm^{-2} current density with KOH), all LCOs showed the attenuated intensity at the (i) shakedown signal (7716~7722) eV and the blue shift of the (ii) white line (7726~7732 eV) denoting 1s $\rightarrow$ 4p transition. These behaviors demonstrated the oxidation of Co^{3+} to Co^{4+}.[12-15] The high magnification of pre-edge regions in 7707~7715 eV is shown in **Figure S10**.

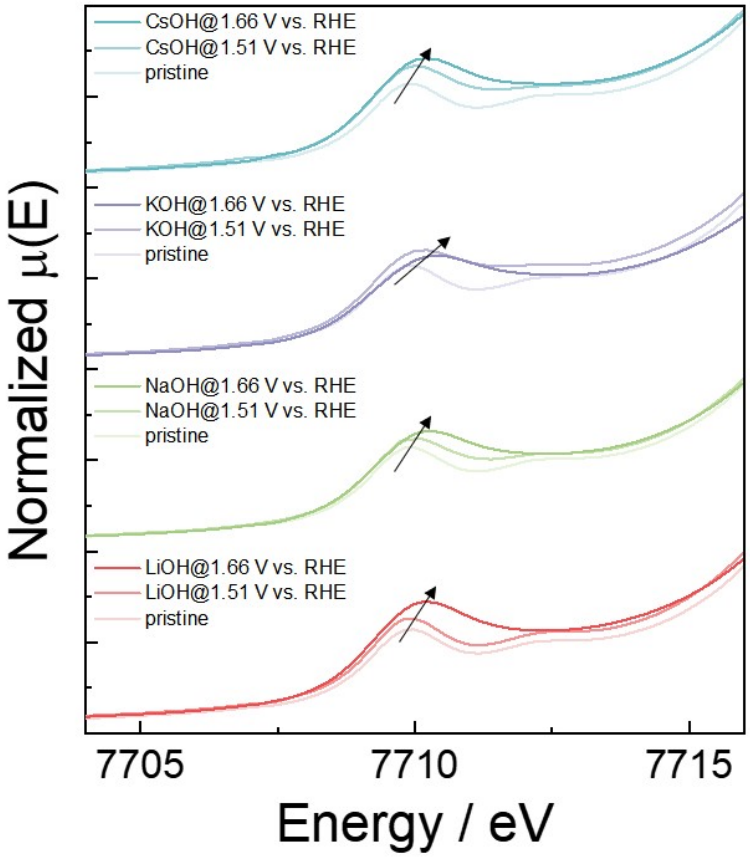

Figure S10. High magnification of the pre-edge region of Co *K* edge XANES spectra. All m-LCOs with alkali metal ion solutions commonly displayed the increased forbidden 1s → 3d transition signals and the blue shift from 1.51 V to 1.66 V vs. RHE, indicating local distortion of CoO_2 layers as forming Co^{4+}.[15]

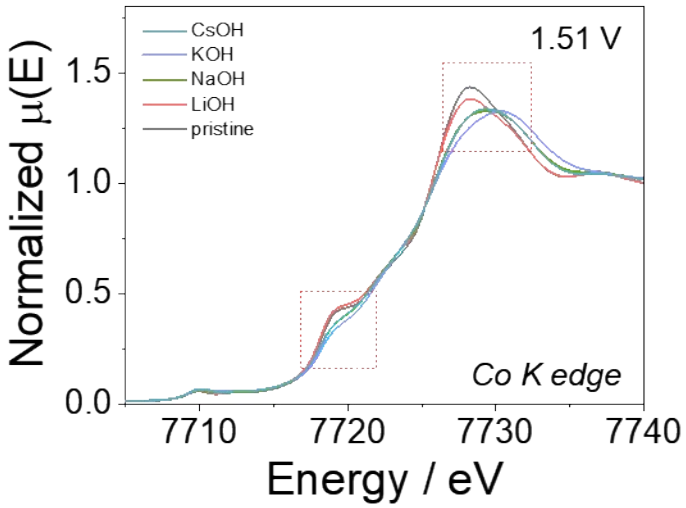

Figure S11. Co *K* edge XANES spectra with different electrolyte solutions after OER at 1.51 V vs. RHE for 60 min. The order of the Co valence states was LiOH < CsOH ≤ NaOH < KOH .

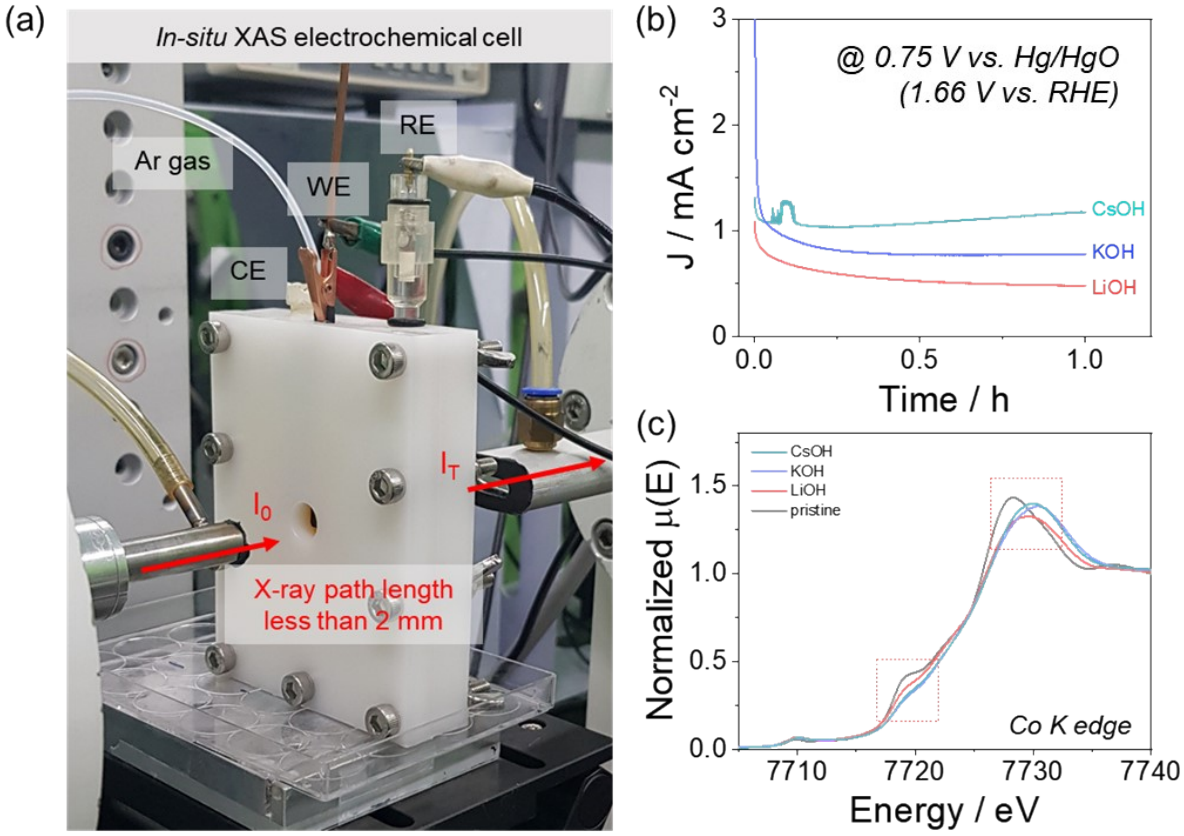

Figure S12. *In situ* measurements of XANES for m-LCOs during 60 min OER at 1.66 V vs. RHE. (a) Digital photo of *in situ* electrochemical XANES cell. Pt wire and Hg/HgO (1 M NaOH) were served as CE and RE, respectively. (b) Chronoamperometric curves with LiOH (red), KOH (blue), and CsOH (cyan) examined after 20 min of Ar-gas bubbling. (c) *In situ* Co *K* edge XANES spectra with the transmission mode, showing the similar propensity of the Co valence state to the above *ex situ* XANES results.

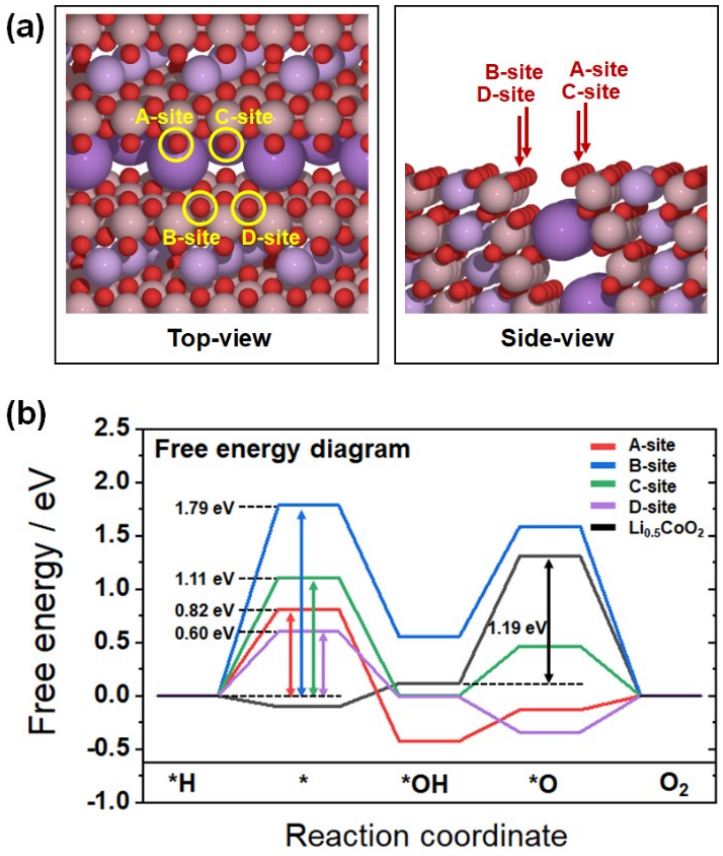

Figure S13. DFT calculations of (012) surface of K^+-intercalated and undoped $Li_{0.5}CoO_2$. (a) Top-view (left panel) and side-view (right panel) of the optimized (012) structures of partially K^+-intercalated $Li_{0.5}CoO_2$. (b) The free energy diagrams for OER at 1.23V vs. RHE on partially K-doped $Li_{0.5}CoO_2$ for four plausible adsorbate sites (red for A-site, blue for B-site, green for C-site, and purple for D-site) compared with undoped $Li_{0.5}CoO_2$ (black).

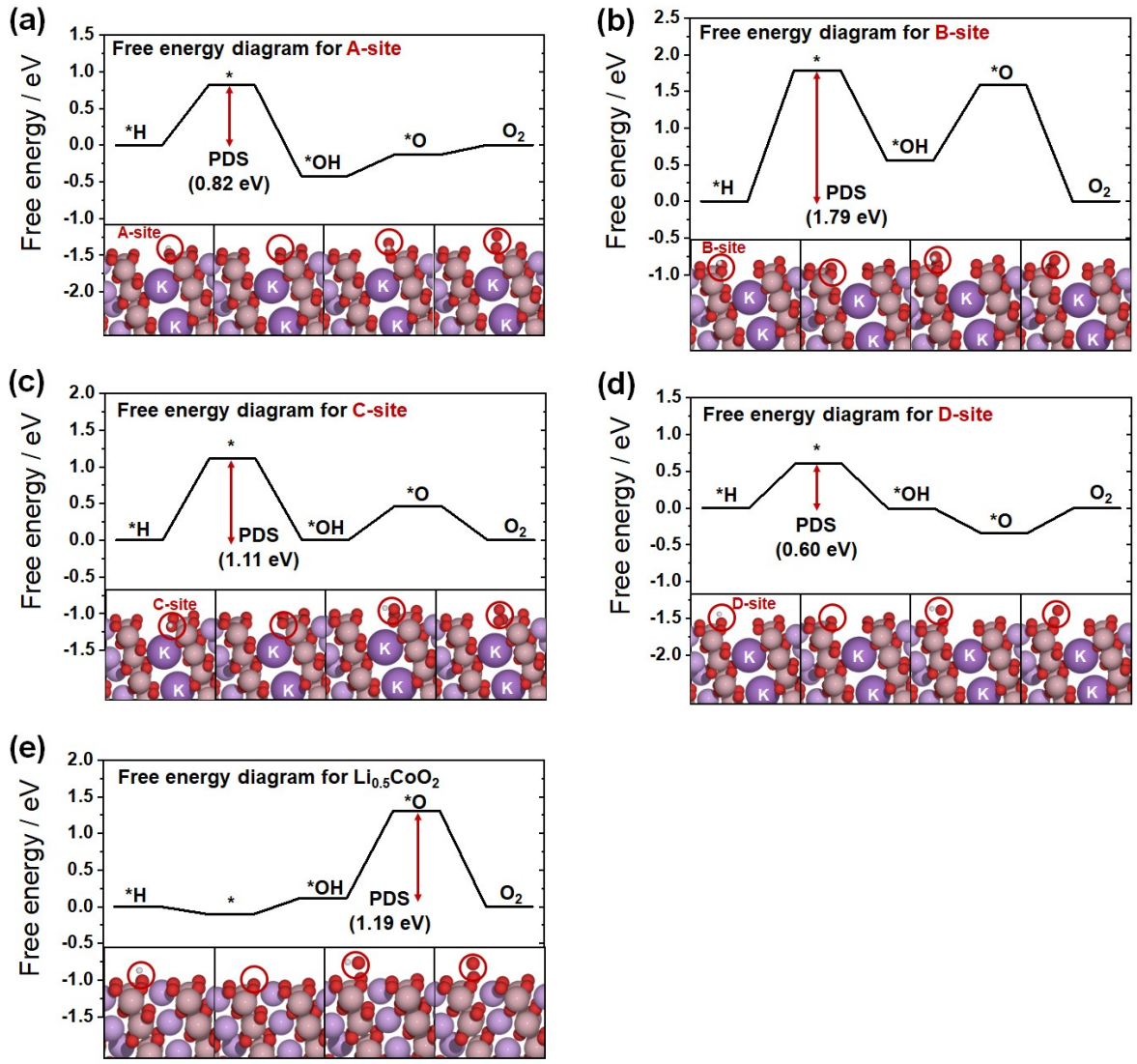

Figure S14. DFT calculations of free energy diagrams showing the reaction pathways for A~D sites of K^+-intercalated $Li_{0.5}CoO_2$ on the (012) structure (top panel) and the corresponding side-views of (012) surfaces aligned with reaction coordinate (bottom panels). (a–d) The free energy diagrams for OER at 1.23 V vs. RHE on partially K^+-intercalated $Li_{0.5}CoO_2$ for plausible adsorbate sites, denoted as A, B, C, and D-sites, respectively. (e) Comparative free energy diagram for undoped $Li_{0.5}CoO_2$.

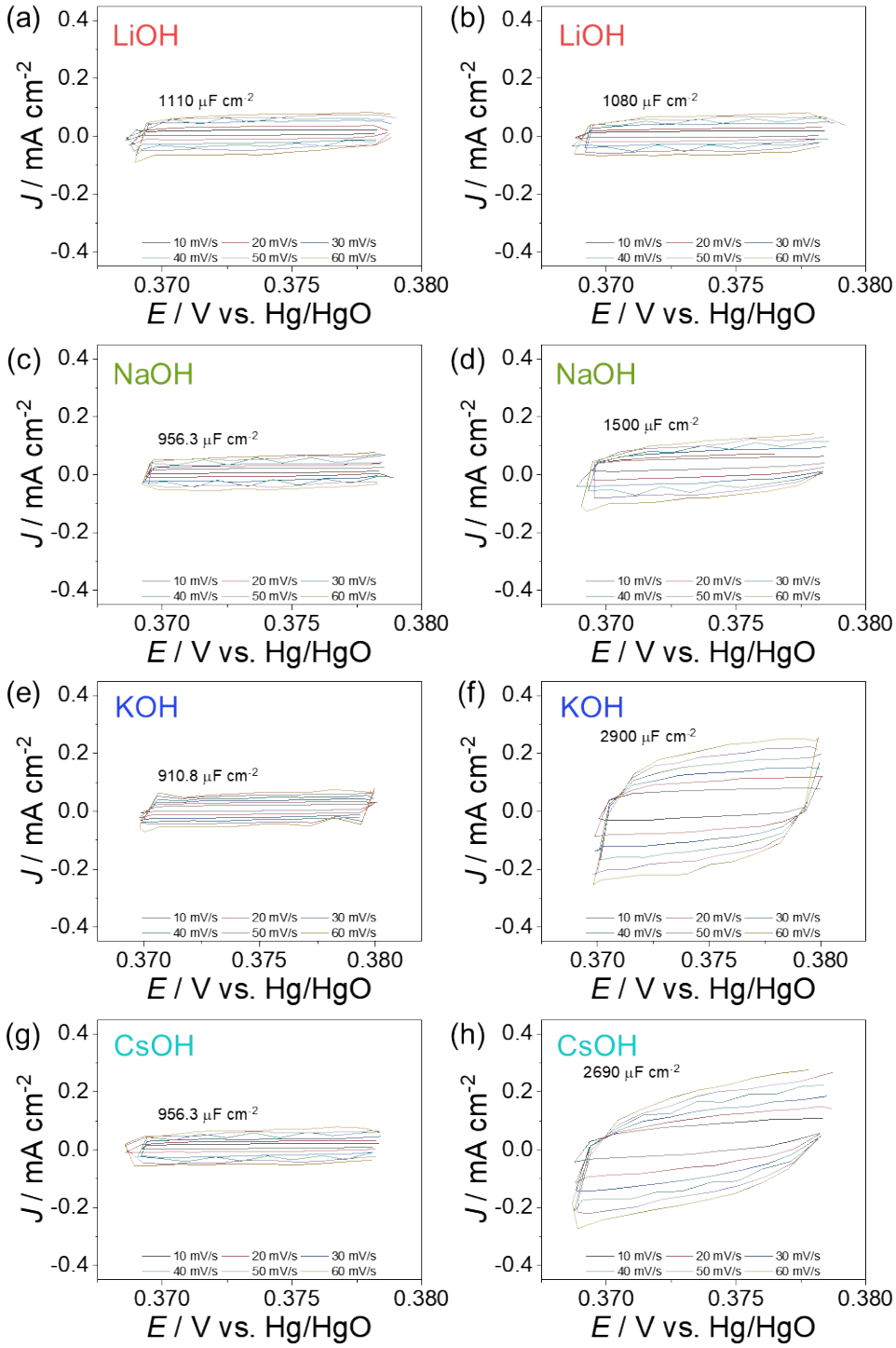

Figure S15. Representative capacitances curves of n-LCO in the potential range of 0.37~0.38 V vs. Hg/HgO with 0.1 M of (a, b) LiOH, (c, d) NaOH, (e, f) KOH, and (g, h) CsOH. Left (a, c, e, and g) and right columns (b, d, f, and h) of CV curves indicted *before* and *after* OER tests, respectively. Scan rates were 10~60 mV s^{-1}. The point of zero charge of the LCO typically appeared less than 0.15 V vs. Hg/HgO under the Ar-bubbling condition. The electrical double-layer capacitances (EDLCs) before and after OER tests were estimated to be 1110/1080, 956/1500, 911/2900, and 956/2690 μF cm^{-2} for LiOH, NaOH, KOH, and CsOH, respectively.

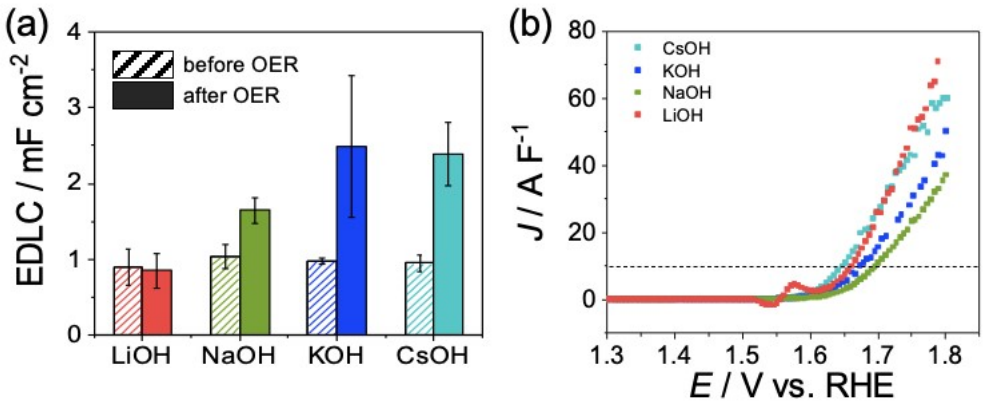

Figure S16. Comparative EDLC values and EDLC-corrected polarization curves. (a) Average EDLCs of n-LCOs before and after OER tests. (b) EDLC-corrected *I*–*E* polarization curves from **Figure 1a**. The current normalized by EDLC revealed that the LCOs with NaOH and KOH provided higher overpotentials than the ones with LiOH at 10 A F^{-1}. However, the LCO with CsOH still had superior OER activity.

The enhanced EDLCs with NaOH, KOH, and CsOH were presumably attributed to the widened CoO_2 interlayers and the increased electronic conductivity.[16, 17] For the former case, the improved EDLC results may be attributed to adsorption of OH^- in the new phases (along with the cation and water in alkaline solutions) and the cracks of the catalysts. However, because these inner basal planes as the new phases do not participate in the OER process, the increased EDLC is not in line with the enlarged active catalytic sites.[1] The latter condition may be achieved if the cation insertion modulates the electronic structure.

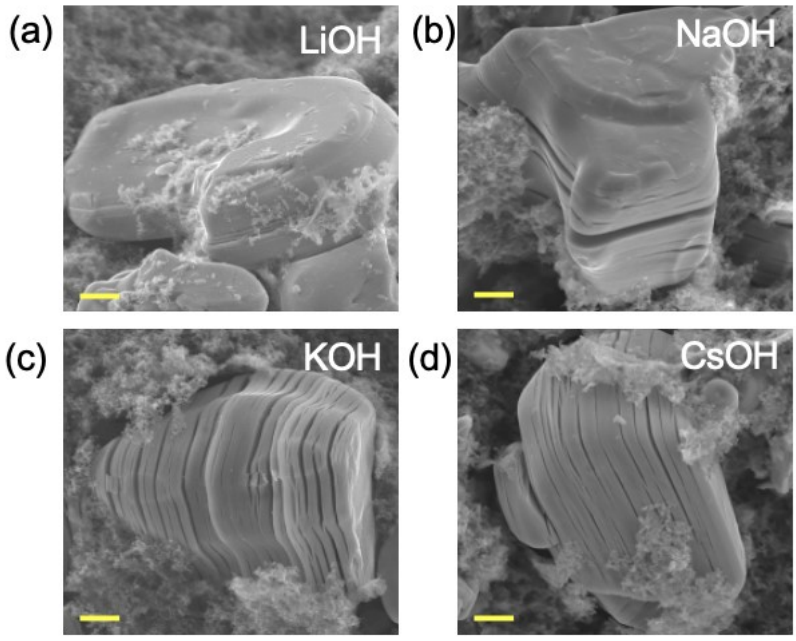

Figure S17. SEM images of m-LCOs with 0.1 M (a) LiOH, (b) NaOH, (c) KOH, and (d) CsOH solution after 90 min OER at 1.65 V vs. RHE. Cracks were developed by intercalating Na^+, K^+, and Cs^+. There was no crack with LiOH(aq). All scale bars indicate 2 μm

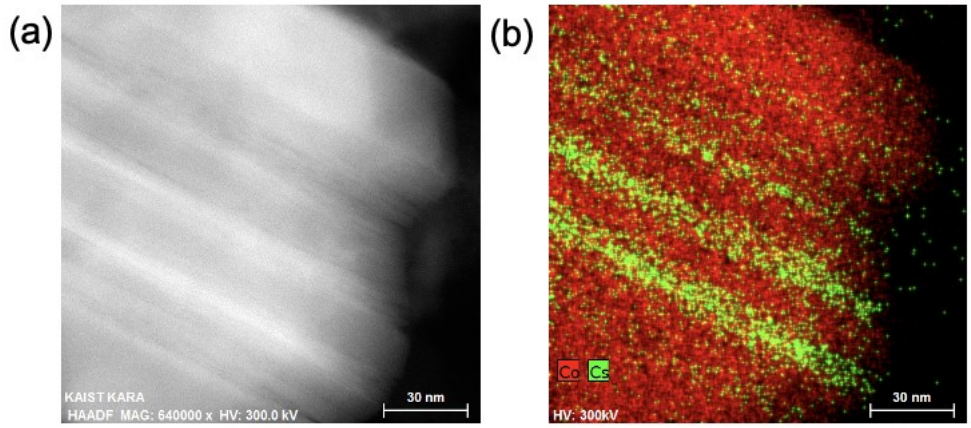

Figure S18. Deep Cs^+ intercalation into the n-LCO using (a) HAADF-STEM images and (b) corresponding elemental mapping images with Co (red) and Cs (green) after 20 min of OER with 0.1 M CsOH at 1.66 V vs. RHE. Only a few new phases were comprising of Cs^+ over the n-LCO, in good agreement with a weak signal of the new phase in the XRD analysis (**Figure 2a** and **Figure S4**).

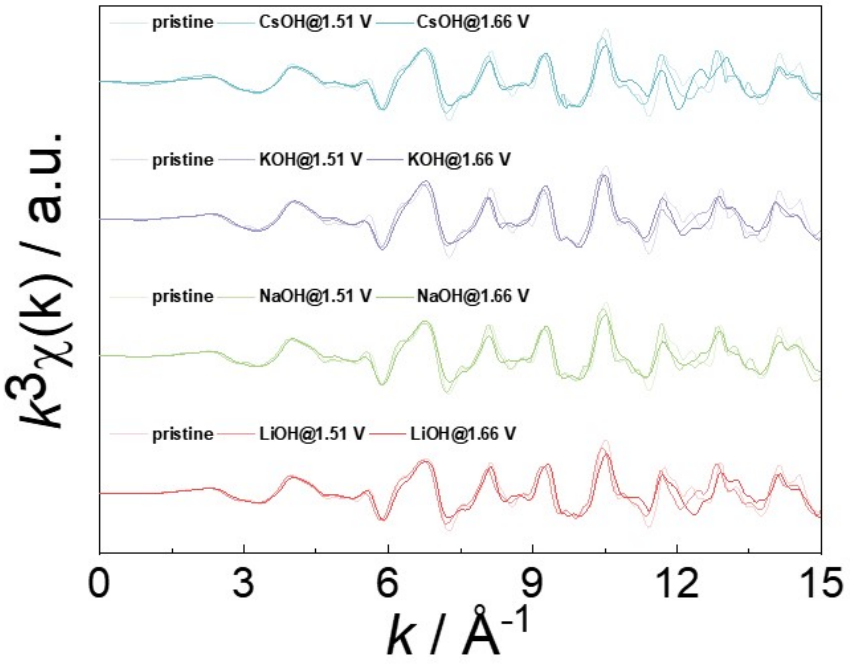

Figure S19. k^3 weighted *ex-situ* Co K edge EXAFS spectra of m-LCO after 60 min of OER at 1.51 V and 1.66 V vs. RHE with different electrolyte solutions.

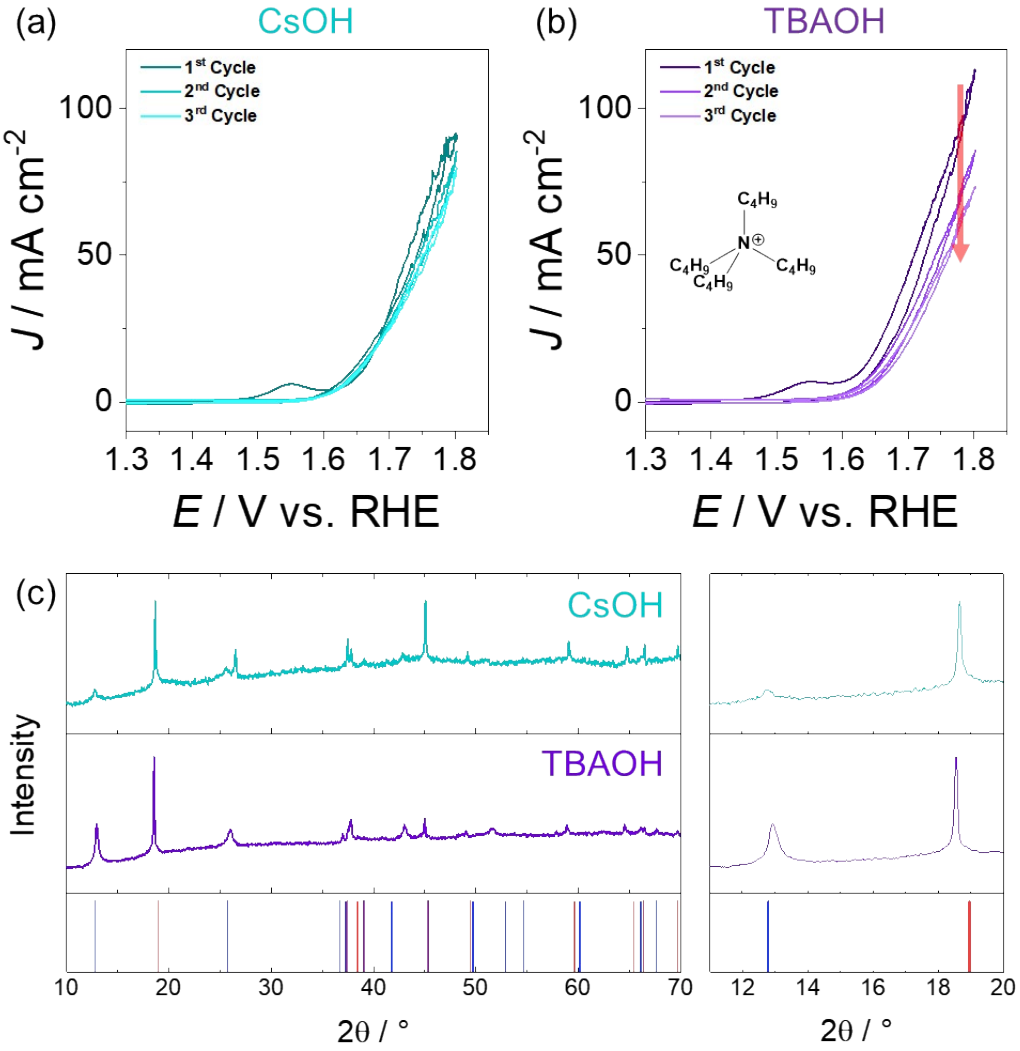

Figure S20. CV tests and XRD analyses of n-LCO with 0.1 M (a) CsOH and (b) tetrabutyl ammonium hydroxide (TBAOH) electrolyte at a scan rate of 10 mV s^{-1}. The n-LCOs with TBAOH exhibited slightly higher OER activity than CsOH at the 1st cycle. However, rapid decay was observed with TBAOH during 3 CV cycles. (c) Powder XRD patterns of m-LCO after 60 min of OER at 1.66 V vs. RHE. Bar patterns in the bottom panel are the references of the layered LCO (red) and $K_{0.3}CoO_2(H_2O)_{0.4}$ (blue). The left and right panels are wide-angle views (10~80°) and the high-magnification region at 11.5~20 ° region, respectively. The new-phase signals, appearing at 12.7° by TBA^+ intercalation, were more intense than the ones by Cs^+.

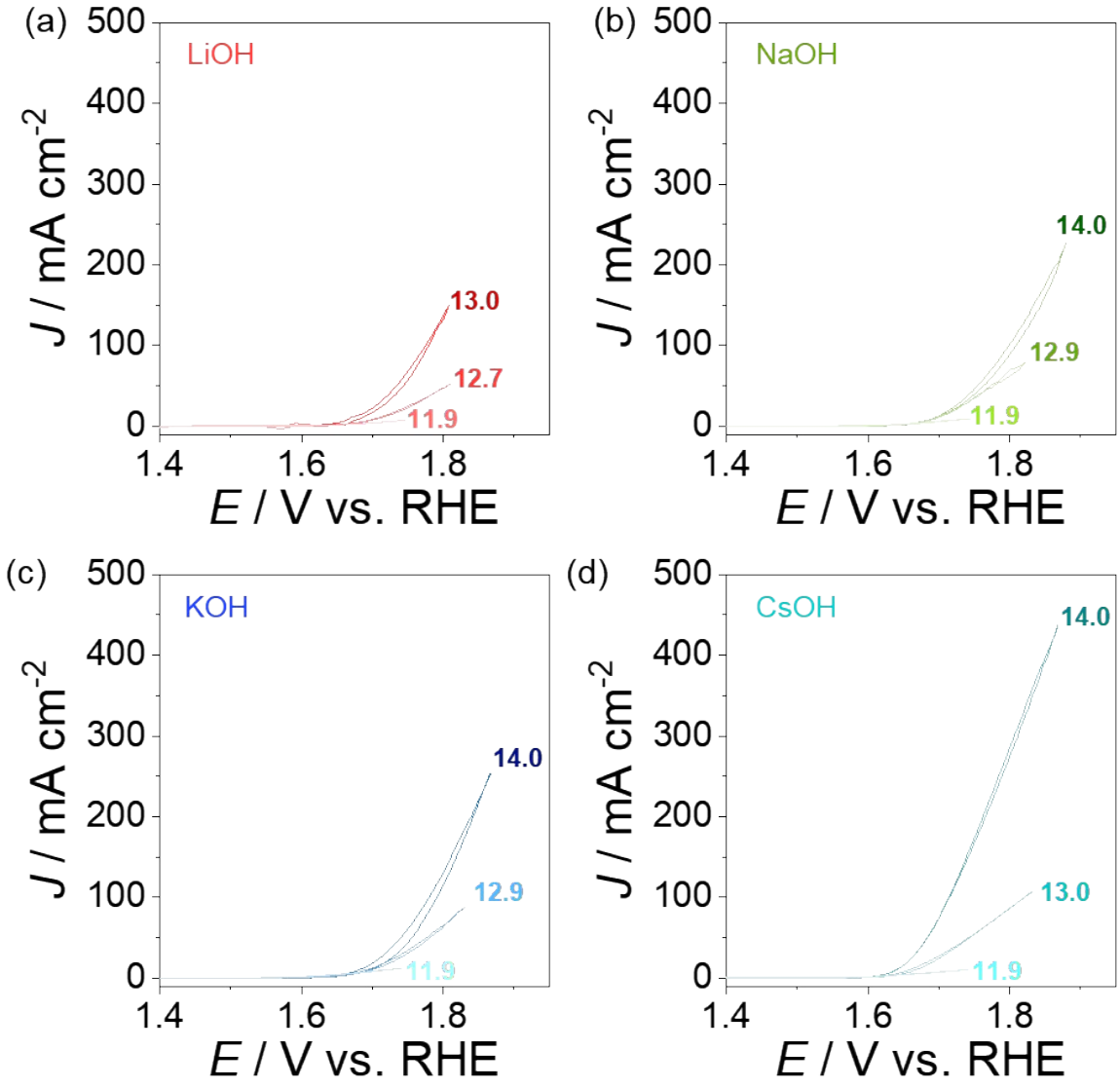

Figure S21. OER polarization curves of n-LCO at pH 12~14 with (a) LiOH, (b) NaOH, (c) KOH, and (d) CsOH. The scan rate was 10 mV s^{-1}. The electrolyte solutions with pH 12, 13, and 14 were prepared by the addition of 10 mM, 100 mM, and 1 M of each electrolyte, respectively.

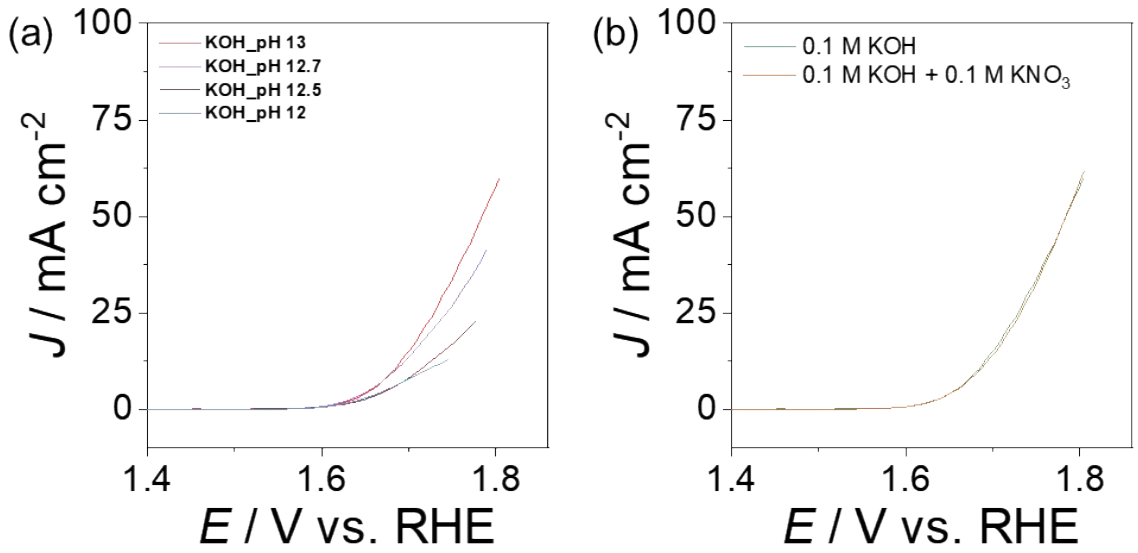

Figure S22. OER polarization curves of n-LCO with KOH electrolyte solutions at the scan rate of 10 mV s^{-1}. (a) All electrolyte solutions contained the constant 0.1 M K^+ concentration regardless of pH, by mixing 0.1 M KOH and 0.1 M KNO_3 with a ratio of 10:0, 5:5, 3:7, and 1:9 to prepare pH 13, 12.7, 12.5, and 12, respectively. (b) Both of electrolytes have same concentration of OH^-, but different K^+ concentration adjusted by adding KNO_3 in 0.1 M KOH. These results suggest OER activity of n-LCO is independent from cation concentration

References

1. Z. Lu, G. Chen, Y. Li, H. Wang, J. Xie, L. Liao, C. Liu, Y. Liu, T. Wu, Y. Li, A. C. Luntz, M. Bajdich and Y. Cui, *J. Am. Chem. Soc.*, 2017, **139**, 6270-6276.
2. S. Zhang, S. Gu, Y. Wang, C. Liang, Y. Yu, L. Han, S. Zheng, N. Zhang, X. Liu, J. Zhou and J. Li, *ACS Catal.*, 2019, **9**, 7389-7397.
3. J. Wang, L. Li, H. Tian, Y. Zhang, X. Che and G. Li, *ACS Appl. Mater. Interfaces.*, 2017, **9**, 7100-7107.
4. Z. Zhang, C. Liu, C. Feng, P. Gao, Y. Liu, F. Ren, Y. Zhu, C. Cao, W. Yan, R. Si, S. Zhou and J. Zeng, *Nano Lett.*, 2019, **19**, 8774-8779.
5. Y. Zhu, W. Zhou, Y. Chen, J. Yu, M. Liu and Z. Shao, *Adv. Mater.*, 2015, **27**, 7150-7155.
6. J. Wang, S.-J. Kim, J. Liu, Y. Gao, S. Choi, J. Han, H. Shin, S. Jo, J. Kim, F. Ciucci, H. Kim, Q. Li, W. Yang, X. Long, S. Yang, S.-P. Cho, K. H. Chae, M. G. Kim, H. Kim and J. Lim, *Nat. Catal.*, 2021, **4**, 212–222.
7. C. Yang, G. Rousse, K. Louise Svane, P. E. Pearce, A. M. Abakumov, M. Deschamps, G. Cibin, A. V. Chadwick, D. A. Dalla Corte, H. Anton Hansen, T. Vegge, J. M. Tarascon and A. Grimaud, *Nat. Commun.*, 2020, **11**, 1378.
8. K. Y. Chung, W.-S. Yoon, H. S. Lee, J. McBreen, X.-Q. Yang, S. H. Oh, W. H. Ryu, J. L. Lee, W. I. Cho and B. W. Cho, *J. Power Sources*, **2006**, **163**, 185-190.
9. T. Maiyalagan, K. A. Jarvis, S. Therese, P. J. Ferreira and A. Manthiram, *Nat. Commun.*, **2014**, **5**, 3949.
10. D. C. L. R. J. Gummow, and M. M. Thackeray, *Mater. Res. Bull.*, **1993**, **28**, 235.
11. Y. Shao-Horn, S. A. Hackney, A. J. Kahaian and M. M. Thackeray, *J. Solid State Chem.*, **2002**, **168**, 60-68.
12. Y.-N. Zhou, J.-L. Yue, E. Hu, H. Li, L. Gu, K.-W. Nam, S.-M. Bak, X. Yu, J. Liu, J. Bai, E. Dooryhee, Z.-W. Fu and X.-Q. Yang, *Adv. Energy. Mater.*, 2016, **6**.
13. F. Alamgir, E. Strauss, S. Greenbaum, J. Whitacre, C.-C. Kao and S. J. J. o. T. E. S. Neih, *J. Electrochem. Soc.*, 2005, **152**, A845-A849.
14. W.-S. Yoon, K.-B. Kim, M.-G. Kim, M.-K. Lee, H.-J. Shin, J.-M. Lee, J.-S. Lee and C.-H. Yo, *J. Phys. Chem. B*, 2002, **106**, 2526-2532.
15. C. J. Patridge, C. T. Love, K. E. Swider-Lyons, M. E. Twigg and D. E. Ramaker, *J. Solid. State. Chem.*, 2013, **203**, 134-144.
16. M. Ménétrier, I. Saadoune, S. Levasseur and C. Delmas, *J. Mater. Chem.*, **1999**, **9**, 1135-1140.
17. Z. Lu, H. Wang, D. Kong, K. Yan, P.-C. Hsu, G. Zheng, H. Yao, Z. Liang, X. Sun and Y. Cui, *Nat. Commun.*, 2014, **5**, 4345.